AIAA SciTech Forum
8–12 January 2018, Kissimmee, Florida
2018 AIAA Guidance, Navigation, and Control Conference

10.2514/6.2018-0384

Design, Implementation and Flight-Test of Incremental Backstepping Flight Control Laws

Wim van Ekeren *, Gertjan Looye †, Richard Kuchar ‡, Qiping Chu §,
Erik-Jan van Kampen ¶

Delft University of Technology, P.O. Box 5058, 2626HS Delft, The Netherlands

DLR, German Aerospace Center, 82234 Weßling, Germany

This paper presents the design and implementation of incremental backstepping (IBS) flight control laws for the attitude control and stabilization on a fixed-wing aircraft. The design consists of multiple functionalities such as command-filtered backstepping, angle of attack control and body attitude control, that are based around an incremental control inner loop that tracks the angular rates of the aircraft. The results include flight data of an integrated IBS design that validate simulation results of control laws shown previously in literature. The results show that it is possible to implement robust nonlinear flight control laws that are easy to tune and require only little knowledge about the system dynamics parameters.

Nomenclature

C_D, C_Y, C_L	Non-dimensional aerodynamic drag, lift and side force	$\mathbf{x}$	Total aircraft state
C_l, C_m, C_n	Non-dimensional aerodynamic roll, pitch and yaw moment	z	Tracking error, $x - x_r$
C_i	Stabilizing control gain matrix in loop i	α	Aerodynamic angle of attack, rad
g	Gravitational acceleration, $^{m}/_{s^2}$	β	Aerodynamic angle of sideslip, rad
I	Aircraft inertia matrix	$\boldsymbol{\omega}$	Aircraft angular rates (in body frame), $^{rad}/_{s}$
m	Aircraft mass, m	ω	Filter bandwidth $^{rad}/_{s}$
$S(\cdot)$	Saturation function	*Subscripts*	
$\mathbb{T}_{ij}$	Coordinate transformation matrix from frame j to frame i	a	Aerodynamic
T_s	Controller sample time, s	act	Actuator
$\mathbf{V}$	Aircraft inertial velocity, $^{m}/_{s}$	b	Body reference frame
V_i	Control Lyapunov Function in step i	m	Measurement
		i	Inertial
		ref	Reference

I. Introduction

Current flight control techniques are most often based on classical control, but modern methods such as nonlinear dynamic inversion (NDI) find more and more applications.[1,2] However, in case of severe or unforeseen failures that change the aircraft behavior (e.g. icing), control systems revert to degradation modes or even direct control. This implies that control law functionality is partly reduced or abandoned.[3] This is unwanted, as in such cases the pilot work load is not only increased due to the failure, but also due to

*Graduate Student, Faculty of Aerospace Engineering, Control and Simulation Division, Delft University of Technology
†Head, Department of Aircraft Systems Dynamics, Institute of System Dynamics and Control, German Aerospace Center
‡Research Associate, Department of Aircraft Systems Dynamics, Institute of System Dynamics and Control, German Aerospace Center
§Associate Professor, Faculty of Aerospace Engineering, Control and Simulation Division, Delft University of Technology
¶Assistant Professor, Faculty of Aerospace Engineering, Control and Simulation Division, Delft University of Technology

aircraft control. Therefore, the objective is to maintain functionality of control systems even in case of such failures. This goal has led to research in the field of reliable fault detection and diagnosis and in the field of control reconfiguration.[3,4] One aspect in this research is the adaptation of flight control laws to unforeseen circumstances and failures.

NDI and backstepping are attractive control techniques, first of all because they are nonlinear and model-based and do not require gain scheduling. They can provide entirely decoupled control over the entire flight envelope. Secondly, in these control laws it is also clear which parts and parameters need to be adapted in case of changed aircraft behavior. The problem however is that failures and model changes need to be completely identified online.

Incremental nonlinear dynamic inversion (INDI) and incremental backstepping (IBS) are methods that have the same advantages, but attempt to solve the identification problem by reducing its model-dependency. By combined and synchronous measurement (or estimation) of control deflection and angular accelerations, the required model knowledge is reduced to only the control effectiveness and inertia parameters. Implementation was initially considered problematic, but by the aforementioned synchronization, the control laws run reliably in current control computers at common sampling rates.

Previous work

The essential idea of incremental nonlinear control laws consists of a reformulation of (part of) the system dynamics. This reformulation was first used as a simplified nonlinear dynamic inversion technique,[5,6] and later more formally proposed by Sieberling et al. as incremental nonlinear dynamic inversion (INDI).[7] The method has primarily been used for angular rate tracking and is applied to fixed-wing aircraft, spacecraft, quadcopters and helicopters.[8–11]

When stability must be guaranteed for the cascaded nonlinear control systems, the Lyapunov-based backstepping procedure is a more promising method. The incremental descriptions were first applied to the backstepping control procedure by Acquatella et al.[12,13] Using backstepping control, adaptation strategies of model parameters are derived such that stability can still be guaranteed.[14–17]

INDI as presented by Sieberling et al.[7] was tested in-flight for the first time on the FASER unmanned aerial vehicle (UAV) by German Aerospace Center (DLR) and Delft University of Technology at the University of Minnesota.[18] Other examples of successful real flight-tests with INDI are reported.[9,19] This paper presents flight test results with an IBS flight control law on the same FASER UAV platform at DLR. IBS flight control laws have not been tested before in-flight.

Contribution

The main contribution is to present a complete IBS control design and prove the applicability on a fixed-wing aircraft, supported with real flight-test results. The aircraft used for these flight-tests is the FASER UltraStick120 aircraft, a 2 m span UAV.[20] Tests were performed on a platform operated by DLR. The longitudinal mode of the controllers can either track the pitch angle θ, suitable for manual flight, or the angle of attack α, which is more useful for an outer loop autopilot controller or high-performance aircraft. The lateral mode of the controllers will control the roll angle ϕ while minimizing the side slip angle β and the aerodynamic side force. The avionics components that are available on this aircraft are relatively cheap and widely available. Therefore, the IBS control laws presented in this paper prove its applicability as a robust, flexible and easy-to-tune control law.

Outline

The structure of this paper is as follows. Section II presents the fixed-wing aircraft model that is used in the design. The incremental flight control laws are derived in section III. Thereafter, section IV discusses the final controller design used on the aircraft. In the remaining part of the paper, sections V and VI, the flight test experiments and results are presented. The paper is concluded in section VII.

II. Aircraft model

The aircraft used in this research is the Ultra-Stick120, a 2 m span remotely piloted fixed-wing aircraft. The platform that is used is part of the FASER project, aiming to develop flight platforms with similar hardware and software to make the process of implementing and testing new flight control algorithms as simple as possible. Windtunnel tests are performed to generate a high-fidelity aerodynamic model. Basic properties of the aircraft are listed in Table 1.

Table 1. Basic aircraft parameters of the Ultra-Stick120 platform[1].

Parameter		
Mass (take-off weight)	m	8.13 kg
Length		1.26 m
C.G. from firewall	x_{cg}	0.315 m
Aero ref from firewall	x_a	0.320 m
Roll inertia	I_x	1.031 kgm^2
Pitch inertia	I_y	1.21 kgm^2
Yaw inertia	I_z	2.05 kgm^2
Roll-yaw inertia	I_{xz}	0.433
Chord	$\bar{c}$	0.433 m
Span	b	1.92 m
Wing Area	S	0.769 m^2

[1]Mass moment of inertia parameters were adopted from the already available model and scaled by the updated operational weight as used by the DLR

A. Equations of motion

The motion of the aircraft is described by rigid-body equations of motion in the body reference frame, as is common in many flight control problems. The most important assumptions made are:

- The aircraft is treated as a rigid body.
- The earth is flat and non-rotating, so that the north-east-down (NED) earth-fixed reference frame is inertial and the gravity vector always points downwards.
- The only forces and moments acting on the aircraft are aerodynamics, propulsive forces and moments and the aircraft's weight. The propeller thrust F_T acts purely in the direction of the body x-axis.
- The mass m of the aircraft is constant.

By applying Newton's equations of motion in the body reference frame, the time derivative of the body velocities $\mathbf{V} = [u, v, w]^T$ are defined as

$$\dot{\mathbf{V}} = \frac{\mathbf{F}_a}{m} + \frac{\mathbf{F}_p}{m} + \mathbf{g} - \boldsymbol{\omega} \times \mathbf{V} \tag{1}$$

where $\boldsymbol{\omega} = [p, q, r]^T$ are the rotational rates and $\mathbf{F}_a, \mathbf{F}_p$ are the aerodynamic and propeller/motor forces respectively, and $\mathbf{g}$ is the gravitational acceleration in body frame coordinates. The terms are given by

$$\mathbf{F}_a = \begin{bmatrix} \bar{X}_b \\ \bar{Y}_b \\ \bar{Z}_b \end{bmatrix} = \mathbb{T}_{bs}(\alpha)\bar{q}S \begin{bmatrix} -C_D \\ C_Y \\ -C_L \end{bmatrix}, \quad \mathbf{F}_p = \begin{bmatrix} F_T \\ 0 \\ 0 \end{bmatrix}, \quad \mathbf{g} = \mathbb{T}_{be}(\phi, \theta, \psi) \begin{bmatrix} 0 \\ 0 \\ g \end{bmatrix} = \begin{bmatrix} -g \sin\theta \\ g \cos\theta \sin\phi \\ g \cos\theta \cos\phi \end{bmatrix}, \tag{2}$$

where $\bar{q} = \frac{1}{2}\rho V_a^2 S$ is the dynamic pressure, S is the wing surface area, $\mathbf{C}_F = [C_D, C_Y, C_L]^T$ the non-dimensional aerodynamic force coefficients, g the gravitational acceleration, $\mathbb{T}_{bs}$ is the rotation matrix from the stability to the body frame over the angle of attack α and $\mathbb{T}_{be}$ is the rotation matrix from the NED frame to the body frame using Euler angles ϕ, θ, ψ. The time derivative of the angular rates $\boldsymbol{\omega}$ is described as

$$\dot{\boldsymbol{\omega}} = I^{-1}(\mathbf{M}_a + \mathbf{M}_p - \boldsymbol{\omega} \times I\boldsymbol{\omega}) \tag{3}$$

where I is the inertia matrix and $\mathbf{M}_p$ are the motor and propeller's reaction moments acting on the aircraft body due to the inertia of the motor and propeller. $\mathbf{M}_a$ is the aerodynamic moment, built up by non-dimensional force and moment coefficients in the body reference frame, defined as

$$\mathbf{M}_a = \bar{q}S \begin{bmatrix} b & & \\ & \bar{c} & \\ & & b \end{bmatrix} \mathbf{C}_M \tag{4}$$

with b the aircraft's wing span, $\bar{c}$ the mean chord length and $\mathbf{C}_M = [C_l, C_m, C_n]^T$ the aerodynamic moment coefficients. Note that the aerodynamic moment coefficients are defined in the body frame while the force coefficients are defined in the stability frame.

B. Aerodynamic model

Aircraft aerodynamic forces are described using non-dimensional force and moment coefficients, denoted as $\mathbf{C}_F = [C_D, C_Y, C_L]^T, \mathbf{C}_M = [C_l, C_m, C_n]^T$. Coefficients are modeled by look-up tables using wind-tunnel test data.[20,21] Coefficients are split up in a base part, depending on angle of attack and angle of sideslip α and β, a part dependent on control surface deflections and a part dependent on the rotational rates, so that

$$\begin{aligned} \mathbf{C}_F &= \mathbf{C}_{F,\text{base}}(\alpha,\beta) + \Delta\mathbf{C}_{F,\text{ctrl}}(\boldsymbol{\delta},\alpha,\beta) + \Delta\mathbf{C}_{F,\text{rate}}(\hat{\boldsymbol{\omega}},\alpha,\beta) \\ \mathbf{C}_M &= \mathbf{C}_{M,\text{base}}(\alpha,\beta) + \Delta\mathbf{C}_{M,\text{ctrl}}(\boldsymbol{\delta},\alpha,\beta) + \Delta\mathbf{C}_{M,\text{rate}}(\hat{\boldsymbol{\omega}},\alpha,\beta) \end{aligned} \tag{5}$$

with $\hat{\boldsymbol{\omega}} = [\frac{pb}{2V_a}, \frac{q\bar{c}}{2V_a}, \frac{rb}{2V_a}]^T$. Coefficients are measured at high angles of attack ($-2 \leq \alpha \leq 45$deg) and angles of sideslip ($-30 \leq \beta \leq 30$deg). Also, control moments $\mathbf{C}_M(\delta)$ and dynamic moments $\mathbf{C}_M(p,q,r)$ are incorporated for different angles of attack, for the complete range of control surface deflections and up to $150\,^{\text{deg}}/_{\text{s}}$ (at $V = 25\,^{\text{m}}/_{\text{s}}$).

To obtain estimates of the control effectiveness of the actuators, and to create a flexible, simplified model which is useful for simulation and controller design, the aerodynamic forces and moments are estimated by a polynomial model at angles of attack smaller than the stall angle ($\alpha < 12\,\text{deg}$) and low angles of sideslip ($\beta < 20\,\text{deg}$), according to

$$\begin{bmatrix} \mathbf{C}_F \\ \mathbf{C}_M \end{bmatrix} = \sum_{i=0}^{2}\sum_{j=0}^{2} \mathbf{c}_{\text{base}_{ij}} \alpha^i \beta^j + \mathbf{c}_{\text{base}_{03}} \beta^3 + \sum_{k=1}^{3}\sum_{i=0}^{2}\sum_{j=0}^{2} \mathbf{c}_{\text{ctrl}_{kij}} \delta_k \alpha^i \beta^j + \sum_{l=1}^{3}\sum_{j=0}^{2} \mathbf{c}_{\text{rate}_{lij}} \hat{\omega}_l \alpha^i \beta^j \tag{6}$$

Here, δ_k with $k = 1,2,3$ are the control surface deflections, and $\hat{\omega}_l$ with $l = 1,2,3$ are the non-dimensional angular rates. $\mathbf{c}_{(\ldots)}$ are the polynomial coefficients. The basic estimated stability and control derivatives are stated in Table 2.

Table 2. Most important estimated stability and control derivatives from the look-up table data.

C_{m_α}	C_{n_β}	C_{l_p}	C_{m_q}	C_{n_r}	$C_{l_{\delta_a}}$	$C_{m_{\delta_e}}$	$C_{n_{\delta_r}}$
-0.3025	0.0714	-0.397563	-7.8542	-0.13664	-0.186475	-0.689396	-0.0360641

III. Incremental backstepping control laws

For the control laws that are designed and tested as presented in this paper, two separate control objectives are formulated. The first control objective is the tracking of body attitude Euler angles ϕ, θ. The external tracking commands are ϕ_{cmd} and θ_{cmd}, while the heading rate $\dot{\psi}$ is controlled such that coordinated turns are achieved. The second control objective is the tracking of the angle of attack α and the body roll angle ϕ, while stabilizing the side-slip angle β. This makes the second controller a lift-control device, which is more useful for outer loop flight path control tasks or for high-performance aircraft.[22,23]

This section presents the derivation of IBS control laws that are applied on the two different control problems. The two control laws are derived and presented separately in respectively sections A and B. The IBS procedure that is followed and their resulting control laws are very similar to what is presented by Acquatella et al.[12] and Van Gils et al.[17]

A. Attitude control of body Euler angles

The control task in this attitude control problem is to track references for the body Euler angles ϕ and θ, so that

$$\phi = \phi_{ref} \quad \text{and} \quad \theta = \theta_{ref} \tag{7}$$

We specifically focus on the stabilization of the aircraft attitude angles ϕ and θ and we are not interested in the total heading ψ or course χ. Normally, the aircraft's heading is controlled by rolling the aircraft into a coordinated turn. Hence, although the total heading is not controlled, it is desired to keep a coordinated turn when performing a roll maneuver by commanding yaw rates. It will be shown that due to the kinematic relation between $\dot{\phi}, \dot{\theta}, \dot{\psi}$ and p, q, r, any reference $\dot{\psi}_{ref}$ can always be chosen so that a reference for p, q, r that tracks the pitch and roll references can be defined. In section C a reference for $\dot{\psi}_{ref}$ is designed that

controls the side force on the aircraft to zero and keeps the sideslip angle small. In this section, the output, tracking error, and state of the outer loop are:

$$\mathbf{y}_1 = \begin{bmatrix} \phi \\ \theta \end{bmatrix}, \quad \mathbf{y}_{1,ref} = \begin{bmatrix} \phi \\ \theta \end{bmatrix}_{ref}, \quad \mathbf{z}_1 = \mathbf{y}_1 - \mathbf{y}_{1,ref}, \quad \mathbf{x}_1 = \begin{bmatrix} \phi \\ \theta \\ \psi \end{bmatrix} \tag{8}$$

The state, tracking error and input in the inner loop are:

$$\mathbf{x}_2 = \begin{bmatrix} p \\ q \\ r \end{bmatrix}, \quad \mathbf{z}_2 = \mathbf{x}_2 - \mathbf{x}_{2,ref}, \quad \mathbf{u} = \begin{bmatrix} \delta_e \\ \delta_r \\ \delta_a \end{bmatrix} \tag{9}$$

The references are outputs of a pre-filter to prevent unachievable commands that will saturate the actuators. The pre-filter also provides a time-derivative of the reference signal, which is used for feed-forward control.

1. Dynamics

The output $\mathbf{y}_1$ is related to the state $\mathbf{x}_1$ by

$$\mathbf{y}_1 = \begin{bmatrix} 1 & 0 & 0 \\ 0 & 1 & 0 \end{bmatrix} \mathbf{x}_1 = H_1 \mathbf{x}_1 \tag{10}$$

The dynamics of $\mathbf{x}_1$ are purely kinematic and we can write

$$\dot{\mathbf{x}}_1 = G_1(\mathbf{x}_1)\mathbf{x}_2 \tag{11}$$

with

$$G_1 = \begin{bmatrix} 1 & \sin\phi\tan\theta & \tan\theta\cos\phi \\ 0 & \cos\phi & -\sin\phi \\ 0 & \sin\phi\sec\theta & \cos\phi\sec\theta \end{bmatrix} \tag{12}$$

The dynamics of the angular rates $\mathbf{x}_2$ are stated in Equation (3). The aerodynamic moment $\mathbf{M}_a$ in Equation (3) is split up in a control-dependent and a control-independent part, using Equation (4) and Equation (5)

$$\dot{\mathbf{x}}_2 = \mathbf{f}_2(\mathbf{x}) + \mathbf{g}_2(\mathbf{x}, \mathbf{u}) \tag{13}$$

with

$$\begin{aligned} \mathbf{f}_2(\mathbf{x}) &= I^{-1}\left(\bar{q}S\begin{bmatrix} b & \bar{c} \end{bmatrix}_b \mathbf{C}_{M,\text{base+rate}} + \mathbf{M}_p - \boldsymbol{\omega} \times \mathbf{V}\right) \\ \mathbf{g}_2(\mathbf{x}, \mathbf{u}) &= I^{-1}\bar{q}S\begin{bmatrix} b & \bar{c} \end{bmatrix}_b \Delta\mathbf{C}_{M,\text{ctrl}} \end{aligned} \tag{14}$$

Here, the aerodynamic coefficients are separated into a control-independent part $\mathbf{C}_{M,\text{rate}}$ and a control-dependent part $\Delta\mathbf{C}_{M,\text{ctrl}}$. $\mathbf{x}$ denotes the total aircraft state which also includes aerodynamic speed and attitude. The dynamics of the angular rates can be written in incremental form by considering a Taylor series expansion around a previous point t_0 in the recent past:[7,8,10]

$$\dot{\mathbf{x}}_2 = \dot{\mathbf{x}}_{2,0} + \underbrace{\left(\frac{\partial \mathbf{f}_2(\mathbf{x})}{\partial \mathbf{x}} + \frac{\partial \mathbf{g}_2(\mathbf{x}, \mathbf{u})}{\partial \mathbf{x}}\right)\Bigg|_{\substack{\mathbf{x}=\mathbf{x}_0 \\ \mathbf{u}=\mathbf{u}_0}}}_{F_{2,0}} (\mathbf{x} - \mathbf{x}_0) + \underbrace{\frac{\partial \mathbf{g}_2(\mathbf{x}, \mathbf{u})}{\partial \mathbf{u}}\Bigg|_{\substack{\mathbf{x}=\mathbf{x}_0 \\ \mathbf{u}=\mathbf{u}_0}}}_{G_{2,0}} (\mathbf{u} - \mathbf{u}_0) + \mathcal{O}\big((\mathbf{x} - \mathbf{x}_0)^2, (\mathbf{u} - \mathbf{u}_0)^2\big) \tag{15}$$

Here, $\mathcal{O}(.)$ represents the truncation error of higher order terms. The second term contains the control derivatives. The control effectiveness matrix $G_{2,0}$ is constructed as

$$G_{2,0} = I^{-1}\bar{q}S \begin{bmatrix} 0 & bC_{l_{\delta_r}} & bC_{l_{\delta_a}} \\ \bar{c}C_{m_{\delta_e}} & 0 & 0 \\ 0 & bC_{n_{\delta_r}} & bC_{n_{\delta_a}} \end{bmatrix} \tag{16}$$

in which the non-dimensional control derivatives are obtained from the polynomial model fit described earlier. Equation (15) is written in shorter form as

$$\dot{\mathbf{x}}_2 = \dot{\mathbf{x}}_{2,0} + F_{2,0}\Delta\mathbf{x} + G_{2,0}\Delta\mathbf{u} \tag{17}$$

Under the assumption that $\mathbf{f}_2(\mathbf{x})$ and $\mathbf{g}_2(\mathbf{x},\mathbf{u})$ do not change significantly due to changes of $\mathbf{x}$ in the interval $[t_0, t]$, and that over this same interval the system is linear so that the higher order terms can be neglected, we can use the following approximation for the angular accelerations:

$$\dot{\mathbf{x}}_2 \cong \dot{\mathbf{x}}_{2,0} + G_{2,0}\Delta\mathbf{u} \tag{18}$$

This assumption is the fundamental step in the simplifications for incremental nonlinear control techniques. Because $F_{2,0}$ contains the major part of the system dynamics, neglecting this term makes any derived model-based control law only dependent on $G_{2,0}$. The assumption is best fulfilled in case actuator dynamics are fast and sampling times are high. For practical applications, this is usually not the case, so some influence of the $F_{2,0}$ contribution is to be expected. This is subject of future work. For now, we assume that the contribution is sufficiently small and can be neglected.

Using the incremental description for the system dynamics, control laws can be made for the incremental control input $\Delta\mathbf{u}$ instead of the total control input $\mathbf{u}$. This means that an incremental control $\Delta\mathbf{u}$ will be derived so that the total control is the sum of the increment and the input at a previous point in time, hence $\mathbf{u} = \Delta\mathbf{u} + \mathbf{u}_0$. With incremental control techniques one relies on a synchronization of the inputs with the feedback of the state derivative, so that the incremental description in Equation (18) holds. Therefore, $\mathbf{u}_0$ should be the delayed real control surface deflection. The feedback of the actuator position must include filters and delays that match the delays in the feedback of the state derivative $\dot{\mathbf{x}}_{2,0}$. It was shown previously that this is a correct way to implement the incremental control law when including actuator dynamics with delayed acceleration measurements.[9] In section IV, the design of the delayed actuator feedback will be discussed in detail.

2. Backstepping Procedure

The backstepping procedure applies to systems in strict feedback form, so that states are separated in subsequent integrator steps from the output. The input appears only at the last integrator step. In this case, we convert the tracking problem into a stabilization problem by using the tracking errors $\mathbf{z}_1$. The idea of backstepping is to create stabilizing functions for each subsequent state at a time, using control Lyapunov functions (CLFs). In the last step, one can derive a description of the input $\mathbf{u}$ that proves asymptotic stability of the tracking error $\mathbf{z}_1$ at the equilibrium point $\mathbf{z}_1, \mathbf{z}_2 = 0$ when the time derivative of the final CLF is negative definite. In that case, the CLF is proven to be a Lyapunov function.

Command-filtered backstepping is implemented by using a linear, first-order command filter to calculate a smooth reference $\mathbf{x}_{2,ref}$ from the command value $\mathbf{x}_{2,cmd}$. This makes it unnecessary to calculate the time derivative $\dot{\mathbf{x}}_{2,ref}$ analytically. The bandwidth of this linear filter is high so that it is safe to assume that $\mathbf{x}_{2,ref} = \mathbf{x}_{2,cmd}$. In reality, the effect that this filter has on the tracking error $\mathbf{z}_1$ is estimated with a linear filter and the tracking error $\mathbf{z}_1$ used in the control law is augmented with this estimate to a so-called compensated tracking error. This was also incorporated in the current implementation. For the simplicity of derivation, this part is omitted in the presented derivation. We refer to previously presented studies for a more detailed explanation.[15,17]

The backstepping procedure is started by defining the first CLF as a radially unbounded function in the elements of $\mathbf{z}_1$ as

$$V_1(\mathbf{z}_1) = \frac{1}{2}\mathbf{z}_1^T\mathbf{z}_1 \tag{19}$$

Let the reference $\mathbf{x}_{2,ref}$ satisfy

$$\mathbf{x}_{2,ref} = G_1^{-1}\left(\begin{bmatrix} -C_1\mathbf{z}_1 \\ 0 \end{bmatrix} + \begin{bmatrix} \dot{\mathbf{x}}_{1,ref} \\ \dot{\psi}_{ref} \end{bmatrix}\right) \tag{20}$$

with C_1 being a diagonal matrix with positive definite elements. The error dynamics $\dot{\mathbf{z}}_1$ yield

$$\begin{aligned} \dot{\mathbf{z}}_1 &= \dot{\mathbf{y}}_1 - \dot{\mathbf{y}}_{1,ref} \\ &= H_1G_1(\mathbf{z}_2 + \mathbf{x}_{2,ref}) - H_1\dot{\mathbf{x}}_{1,ref} \\ &= H_1G_1\mathbf{z}_2 - C_1\mathbf{z}_1 \end{aligned} \tag{21}$$

By substition of Equation (21), the time derivative $\dot{V}_1$ yields

$$\begin{aligned}\dot{V}_1 &= \mathbf{z}_1^T \dot{\mathbf{z}}_1 \\ &= -\mathbf{z}_1^T C_1 \mathbf{z}_1 + \mathbf{z}_1^T H_1 G_1 \mathbf{z}_2\end{aligned} \tag{22}$$

Then, $\dot{V}_1$ is negative definite along $\mathbf{z}_1$ except for the second term, due to $\mathbf{z}_2$. This term will be accounted for in the subsequent design step. To start the next and final step of the backstepping procedure, the CLF is augmented by a term that is radially unbounded in the elements of $\mathbf{z}_2$:

$$V_2(\mathbf{z}_1, \mathbf{z}_2) = V_1 + \frac{1}{2}\mathbf{z}_2^T \mathbf{z}_2 \tag{23}$$

In the time derivative $\dot{V}_2$, we substitute for the system dynamics of $\mathbf{x}_2$ in incremental form:

$$\dot{V}_2 = \dot{V}_1 + \mathbf{z}_2^T \left\{ \dot{\mathbf{x}}_{2,0} + G_{2,0} \Delta \mathbf{u} - \dot{\mathbf{x}}_{2,ref} \right\} \tag{24}$$

If the incremental control satisfies

$$\Delta \mathbf{u} = G_{2,0}^{-1} \left(-C_2 \mathbf{z}_2 - \dot{\mathbf{x}}_{2,0} + \dot{\mathbf{x}}_{2,ref} + G_1^T H_1^T \mathbf{z}_1 \right) \tag{25}$$

then the time derivative of the final CLF $\dot{V}_2$ yields

$$\dot{V}_2 = -\mathbf{z}_1^T C_1 \mathbf{z}_1 - \mathbf{z}_2^T C_2 \mathbf{z}_2 \tag{26}$$

with C_1 a diagonal matrix with positive definite elements. This shows that $\dot{V}_2$ is negative definite along $\mathbf{z}_1$ and $\mathbf{z}_2$. The result implies that with the given commands, the equilibrium $\mathbf{z}_1, \mathbf{z}_2 = 0$ is asymptotically stable, which implies that $\mathbf{z}_1, \mathbf{z}_2 \to \mathbf{0}$ when $t \to \infty$. Furthermore, the stabilization problem is exponentially stable in all terms with a decay rate determined by C_1 and C_2, because a positive definite scalar η exists such that

$$\begin{aligned}\dot{V}_2 &= -\mathbf{z}_1^T C_1 \mathbf{z}_1 - \mathbf{z}_2^T C_2 \mathbf{z}_2 \\ &\leq -\eta \left(\frac{1}{2}\mathbf{z}_1^T \mathbf{z}_1 + \frac{1}{2}\mathbf{z}_2^T \mathbf{z}_2 \right) \\ &= -\eta V_2\end{aligned} \tag{27}$$

This concludes the derivation of the stable IBS control law for the body attitude control problem. An overall control diagram is shown in Figure 1.

B. Attitude control of aerodynamic angles

For the backstepping control procedure presented in this section, the aerodynamic attitude of the aircraft is controlled. Controlled variables are

$$\phi = \phi_{ref}, \quad \alpha = \alpha_{ref}, \quad \beta = \beta_{ref} \tag{28}$$

By controlling the aerodynamic attitude, one effectively controls the aerodynamic forces on the aircraft, since at given airspeeds the angle of attack is proportional to the vertical load. This type of control is useful for trajectory control or the attitude control of high-performance aircraft. Simulations with INDI and IBS aerodynamic attitude control laws are successfully shown previously in literature.[11,17,23] The reference β_{ref} is set to zero to approximate a coordinated turn. The output, tracking errors, states and input are now defined as

$$\mathbf{y}_1 = \mathbf{x}_1 = \begin{bmatrix}\phi \\ \alpha \\ \beta\end{bmatrix}, \quad \mathbf{y}_{1,ref} = \mathbf{x}_{1,ref} = \begin{bmatrix}\phi \\ \alpha \\ \beta\end{bmatrix}_{ref}, \quad \mathbf{z}_1 = \mathbf{x}_1 - \mathbf{x}_{1,ref}, \quad \mathbf{x}_2 = \begin{bmatrix}p \\ q \\ r\end{bmatrix}, \quad \mathbf{u} = \begin{bmatrix}\delta_e \\ \delta_r \\ \delta_a\end{bmatrix} \tag{29}$$

Output $\mathbf{y}_1$ equals the state $\mathbf{x}_1$ but has been defined anyway to keep consistent with our notations. Hence, the relationship between $\mathbf{y}_1$ and $\mathbf{x}_1$ is defined as

$$\mathbf{y}_1 = H_1 \mathbf{x}_1, \quad H_1 = I_{3\times 3} \tag{30}$$

1. Dynamics

While the time derivative of ϕ directly follows from the kinematic transformation presented in Equation (11), the time derivative of α and β must be derived from a coordinate transformation of $[u, v, w] \Leftrightarrow [V_c, \alpha_c, \beta_c]$[17,23] and substitution in the equation for the linear accelerations in Equation (1). A subscript c has been explicitly added to denote that the aerodynamic angles are with respect to the inertial constant-wind reference frame, because u, v, w are the inertial body velocities. Hence, they are not relative to the local wind. When considering an inertial frame fixed to the constant horizontal wind component, the equations for $\dot{\alpha}_c$ and $\dot{\beta}_c$ hold. The time derivatives for α_c and β_c yield

$$\begin{aligned}\dot{\alpha}_c &= q - p\cos\alpha_c\tan\beta_c - r\sin\alpha_c\tan\beta_c + \frac{1}{mV_c\cos\beta_c}\big(-A_x\sin\alpha_c + A_z\cos\alpha_c + mg_3\big)\\ \dot{\beta}_c &= p\sin\alpha_c - r\cos\alpha_c + \frac{1}{mV_c}\big(-A_x\cos\alpha_c\sin\beta_c + A_y\cos\beta_c - A_z\sin\alpha_c\sin\beta_c + mg_2\big)\end{aligned} \tag{31}$$

with A_x, A_y, A_z the specific forces that can be measured directly and

$$\begin{aligned}g_2 &= g\left(\cos\alpha_c\sin\beta_c\sin\theta + \cos\beta_c\sin\phi\cos\theta - \sin\alpha_c\sin\beta_c\cos\phi\cos\theta\right)\\ g_3 &= g\left(\sin\alpha_c\sin\theta + \cos\alpha_c\cos\phi\cos\theta\right)\end{aligned} \tag{32}$$

The dynamics can be written in a more general form as

$$\dot{\mathbf{x}}_1 = \mathbf{f}_1(\mathbf{x}, \dot{\mathbf{x}}) + G_1(\mathbf{x})\mathbf{x}_2 \tag{33}$$

with

$$\begin{aligned}\mathbf{f}_1(\mathbf{x}, \dot{\mathbf{x}}) &= \begin{bmatrix} 0 \\ \frac{1}{mV_c\cos\beta_c}\big(-A_x\sin\alpha_c + A_z\cos\alpha_c + mg_3\big) \\ \frac{1}{mV_c}\big(-A_x\cos\alpha_c\sin\beta_c + A_y\cos\beta_c - A_z\sin\alpha_c\sin\beta_c + mg_2\big)\end{bmatrix}\\ G_1(\mathbf{x}_1, \theta) &= \begin{bmatrix} 1 & \sin\phi\tan\theta & \tan\theta\cos\phi \\ -\cos\alpha_c\tan\beta_c & 1 & -\sin\alpha_c\tan\beta_c \\ \sin\alpha_c & 0 & -\cos\alpha_c\end{bmatrix}\end{aligned} \tag{34}$$

The structure differs from the outer loop dynamics in the previous section in Equation (11) because of the extra system dynamics term $\mathbf{f}_1$. This term depends on the state derivative $\dot{\mathbf{x}}$, because accelerations appear in the equations for $\dot{\alpha}_c$ and $\dot{\beta}_c$. The term $\mathbf{f}_1$ is measurable when $A_{x,yz}$ and the aerodynamic attitude V_c, α_c, β_c are available and does only contain kinematic relationships. The state $\mathbf{x}_2$ in Equation (34) are the same body angular rates as in section A which implies that the inner loop dynamics are the same. The same incremental description of Equation (18) therefore also applies here.

2. Backstepping Procedure

The backstepping procedure for this control problem is very similar to the problem defined in the previous section. Again, a fast, unconstrained command filter is used for $\mathbf{x}_{2,ref}$ to obtain a time derivative $\dot{\mathbf{x}}_{2,ref}$. The control Lyapunov function (CLF) is again defined as $V_1 = \frac{1}{2}\mathbf{z}_1^T\mathbf{z}_1$, and the raw intermediate control is defined as

$$\mathbf{x}_{2,ref} = G_1^{-1}\left(-C_1\mathbf{z}_1 - \mathbf{f}_1 + \dot{\mathbf{x}}_{1,ref}\right) \tag{35}$$

with C_1 a diagonal matrix with positive definite elements. The error dynamics yield

$$\begin{aligned}\dot{\mathbf{z}}_1 &= H_1\dot{\mathbf{x}}_1 - H_1\dot{\mathbf{x}}_{1,ref} &&= \mathbf{f}_1 + G_1\mathbf{x}_2 - \dot{\mathbf{x}}_{1,ref}\\ &= \mathbf{f}_1 + G_1(\mathbf{x}_{2,ref} + \mathbf{z}_2) - \dot{\mathbf{x}}_{1,ref}\\ &= -C_1\mathbf{z}_1 + G_1\mathbf{z}_2\end{aligned} \tag{36}$$

Taking the time derivative of V_1 and substituting Equation (36) yields

$$\begin{aligned}\dot{V}_1 &= \mathbf{z}_1^T\dot{\mathbf{z}}_1\\ &= -C_1\mathbf{z}_1 + G_1\mathbf{z}_2\end{aligned} \tag{37}$$

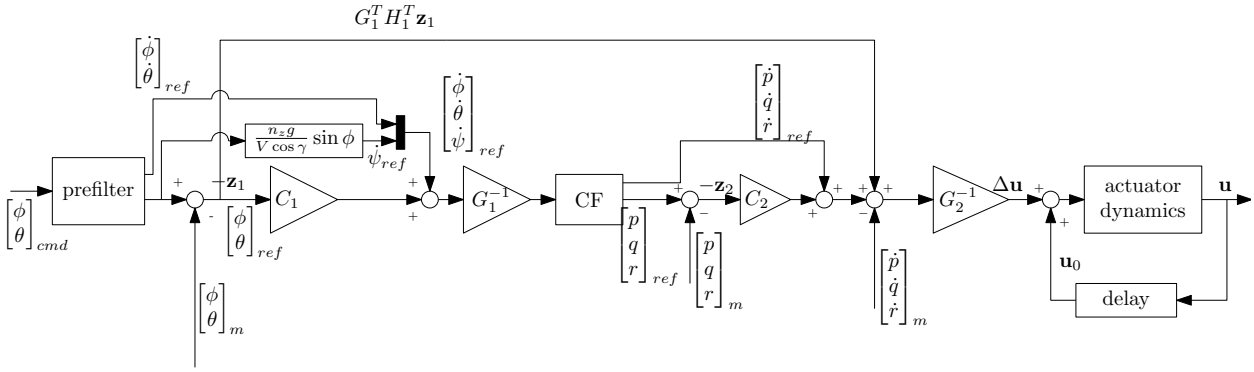

Figure 1. Control structure of the IBS body attitude control law.

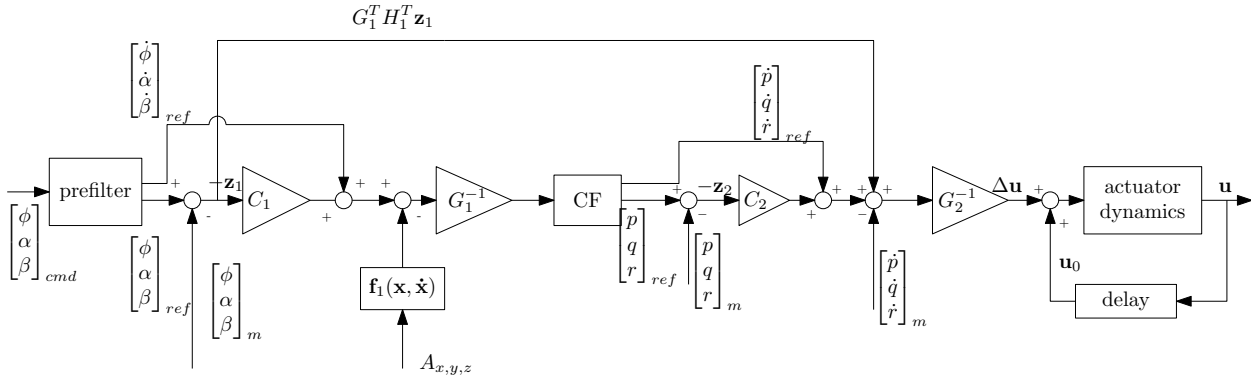

Figure 2. Control structure of the IBS aerodynamic attitude control law. Note that this differs only from the body attitude control law in the outer loop.

The second step of the backstepping is identical to the previous section, except that one has to compensate a different term from the first step, because $\mathbf{z}_1^T G_1$ refers to different physical variables. Hence, augmenting the CLF as $V_2 = V_1 + \frac{1}{2}\mathbf{z}_2^T \mathbf{z}_2$ and selecting the raw incremental control law as

$$\Delta\mathbf{u} = G_{2,0}^{-1}\left(-C_2\mathbf{z}_2 + \dot{\mathbf{x}}_{2,ref} + G_1^T\mathbf{z}_1 - \dot{\mathbf{x}}_{2,0}\right) \tag{38}$$

yields

$$\dot{V}_2 = -\mathbf{z}_1^T C_1 \mathbf{z}_1 - \mathbf{z}_2^T C_2 \mathbf{z}_2 \tag{39}$$

This implies again that $\mathbf{z}_1, \mathbf{z}_2 \to 0$ when $t \to \infty$, and asymptotic stability is obtained. Furthermore, the stabilization problem is exponentially stable in all terms with a decay rate determined by C_1 and C_2, because a positive definite scalar η exist such that

$$\begin{aligned} \dot{V}_2 &= -\mathbf{z}_1^T C_1 \mathbf{z}_1 - \mathbf{z}_2^T C_2 \mathbf{z}_2 \\ &\leq -\eta\left(\frac{1}{2}\mathbf{z}_1^T\mathbf{z}_1 + \frac{1}{2}\mathbf{z}_2^T\mathbf{z}_2\right) \\ &= -\eta V_2 \end{aligned} \tag{40}$$

A schematic of the control law is shown in Figure 2.

C. Remarks on the derived incremental backstepping control laws

1. Linear control laws

The derived control laws in Equations (25) and (38) only contain a proportional feedback of the tracking errors $\mathbf{z}_1, \mathbf{z}_2$ with proportional gains C_1, C_2. In addition to a proportional control law, during the backstepping

procedure one is free to extend the control law with e.g. an integrator $\int \mathbf{z}dt$ or derivative part $\dot{\mathbf{z}}$. Lyapunov stability can still be proven when integrator or derivative control terms are added. During the control design it is common practice to use such extensions, to compensate for differences between the theoretical model and a practical application that includes e.g. actuator dynamics and more complex dynamics.

2. Comparison with multi-loop incremental nonlinear dynamic inversion

The resulting control laws stated in Equations (20), (25), (35) and (38) are very similar to a multi-loop INDI control law. This is interesting to note, because IBS was developed from INDI. An incremental nonlinear dynamic inversion control law for the angular rate tracking problem of fixed-wing aircraft was already shown previously[7] in forms similar to:

$$\Delta\mathbf{u} = G_{2,0}^{-1}\left(\boldsymbol{\nu} - \dot{\mathbf{x}}_{2,0}\right) \tag{41}$$

with $\boldsymbol{\nu}$ a virtual control. The intermediate command $\mathbf{x}_{2,ref}$ identical to Equations (20) and (35) can result from a normal nonlinear dynamic inversion when assuming the angular rates $\mathbf{x}_{2,ref}$ as input in this step. Comparing Equation (41) with Equations (25) and (38), one can see that when the virtual control $\boldsymbol{\nu}$ is set to $-C_2\mathbf{z}_2 + \dot{\mathbf{x}}_{2,ref}$, the IBS differs only by the additional term $G_1^T\mathbf{z}_1$. This term appears in IBS due to the fact that the intermediate reference $\mathbf{x}_{2,ref}$ is not an input but the reference for a state, and hence cannot be reached instantaneously. On the contrary, cascaded nonlinear dynamic inversion control laws need to assume time-scale separation. In normal tracking cases, $G_1^T\mathbf{z}_1$ is very small compared to the virtual control.

3. Adaptation and parameter estimation

The only model parameters that appear explicitly in the nonlinear model-based control laws are the control derivatives and inertia parameters that construct the matrix $G_{2,0}$. These parameters must be identified and adapted upon system faults that change the aircraft behavior. In various previous studies on INDI and IBS, incremental angular rate control was combined with online parameter estimation methods to adapt the matrix $G_{2,0}$.[9,14,24] A simple way to implement adaptation is to use the certainty equivalence principle[25] by treating the estimate $G_{2,0}$ in the control law as the true parameter. On-line identification of $G_{2,0}$ can then be done in a separate, modular way. Because this type of adaption does violate the Lyapunov stability proof, one can use integrated methods such as adaptive backstepping using tuning functions[25] or immersion and invariance[26,27] so that asymptotic stability is guaranteed. This paper does not focus on the estimation or adaptation of $G_{2,0}$. The control laws will use the best off-line estimated control derivatives to construct $G_{2,0}$.

IV. Controller design and implementation

The main control objectives for the controller design are the tracking of the body Euler angles ϕ, θ (the body attitude control law) and alternatively also the tracking of the aerodynamic attitude using α, β, ϕ (the

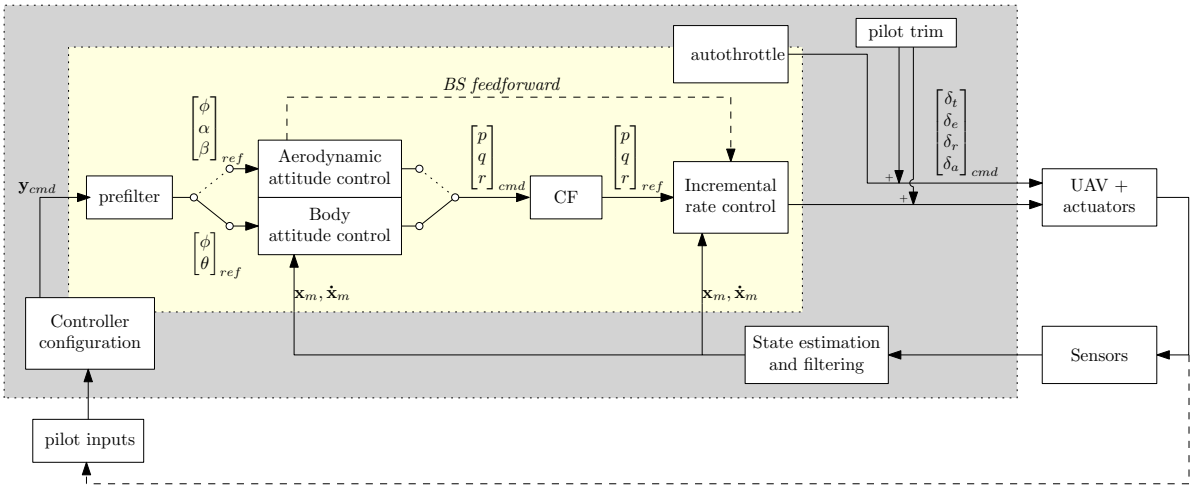

Figure 3. General controller structure at a functional level.

aerodynamic attitude control law). Derivations of the IBS control laws for these objectives were presented in section III.

For a complete controller design that can be tested in flight, one must always consider the characteristics of the specific platform, actuators and sensors, and combine this with appropriate filters and controller parameters to obtain the desired control performance. The most important aspects for this design are discussed in this section. A functional overview of the implemented systems and its main signal interfaces can be found in Figure 3.

A. Pre-filters and command filters

The system dynamics and platform specifications have been assessed and simulated to design a suitable controller that matches the capabilities and limitations of the platform. Pre-filters are first of all implemented to obtain a time-derivative of the command, that is used for the feed-forward control. Secondly, they shape the reference signal such that no unachievable commands are given. Pre-filters for the attitude commands are second-order linear filters with rate and position limits, so that the dynamics for each reference signal are described by

$$\begin{aligned} \begin{bmatrix} q_1(k+1) \\ q_2(k+1) \end{bmatrix} &= \begin{bmatrix} S_M\{q_1(k) + T_s q_2(k)\} \\ q_2(k) + T_s S_R \left\{ 2\zeta\omega_n \left(\frac{\omega_n^2}{2\zeta\omega_n} \left[y_{cmd}(k) - q_1(k) \right] - q_2(k) \right) \right\} \end{bmatrix} \\ y_{ref} &= q_1 \\ \dot{y}_{ref} &= q_2 \end{aligned} \tag{42}$$

with ζ, ω_n the damping and natural frequency of the filter, and S_R and S_M the magnitude and rate limits. Estimates of maximum achievable angular rates and accelerations are used to verify that the pre-filter parameters have conservative settings. Estimates for maximum angular rates and accelerations are calculated using basic estimates of the stability derivatives, e.g.

$$\hat{p}_{max} = \frac{2V}{b} \frac{C_{l_{\delta_a}}}{C_{l_p}} \delta_{a_{max}}, \qquad \hat{\dot{p}}_{max} = -\frac{\bar{q}S}{I_{xx}} C_{l_{\delta_a}} \tag{43}$$

The derivative for α depends both on the pitch rate q and the load factor n_z (see Equation (31)). The maximum rate $\dot{\alpha}_{ref}$ has been determined empirically by finding a conservative limit that yields achievable commands. The dynamics of the command-filters for the angular rate references are a first-order linear filter:

$$x_{ref}(k+1) = x_{ref}(k) + T_s S_R \left\{ \omega_n [x_{cmd}(k) - x_{ref}(k)] \right\} \tag{44}$$

Table 3. Pre-filter parameters and estimated maximum angular rates and accelerations

Ref	$\omega_n[^{\text{rad}}/_{\text{s}}]$	$\zeta[-]$	rate limit $[^{\text{deg}}/_{\text{s}}]$	$\hat{\boldsymbol{\omega}}_{max}[^{\text{deg}}/_{\text{s}}]$	$\hat{\dot{\boldsymbol{\omega}}}_{max}[^{\text{deg}}/_{\text{s}^2}]$
ϕ_{ref}	4	0.7	60	146.8	500.8
θ_{ref}	4	0.7	60	121.5	1571.4
α_{ref}	4	0.7	4		

B. Aerodynamic attitude estimation

On this UAV, no angle of attack or angle of sideslip measurements were available. This is problematic for the aerodynamic attitude controller, since it relies on a feedback of α and β. For this reason, the aerodynamic angles are estimated using the available aerodynamic model. For the angle of attack the simplified aerodynamic lift model is used to estimate α using vertical acceleration measurements:

$$\hat{C}_L = C_{L_0} + C_{L_\alpha}\alpha + C_{L_{\delta_e}}\delta_e, \quad \text{with} \quad \hat{C}_L \bar{q} S \cong -mA_z \cos\alpha \tag{45}$$

This equation is solved for α. For β, lateral accelerations A_y are used:

$$\hat{C}_Y = C_{Y_\beta}\beta + C_{Y_r}\frac{rb}{2V_a}, \quad \text{with} \quad \hat{C}_Y \bar{q} S \cong mA_y \tag{46}$$

When used in real flight, the estimations $\hat{\alpha}$ and $\hat{\beta}$ will contain the experienced turbulence and other vibrations at each particular moment. To prevent the aircraft to create unnecessary control effort by tracking this turbulence and vibrations, the aerodynamic angles must ideally be filtered or estimated in other ways. Following the definitions in Equation (31), the aerodynamic angles should be relative to the constant wind vector. Estimations can be obtained by using e.g. a complementary filter in which the estimations above are the slow component and aerodynamic angles obtained from the inertial velocities are the fast component of the filter. However, at the moment of flight tests, such a filter was not yet implemented and tested. Therefore, the above mentioned estimates $\hat{\alpha}$ and $\hat{\beta}$ are used as feedback.

C. Heading rate reference for coordinated turn maneuvers

From the derived intermediate body attitude control law in Equation (20) it follows that an arbitrary reference $\dot{\psi}_{ref}$ may be defined without affecting the stability of the controlled variables ϕ, θ. Usually for fixed-wing aircraft, a desired heading rate $\dot{\psi}$ or course rate $\dot{\chi}$ determines the required roll angle ϕ. However, in the control problem presented in this paper we are only interested in the control of the roll and pitch angle directly. Therefore, the reference $\dot{\psi}_{ref}$ is derived from the actual roll angle to achieve a coordinated turn. The relationship for the generation of $\dot{\psi}_{ref}$ that is used is:

$$\dot{\psi}_{ref} = \frac{mA_z \sin\phi_{ref}}{V_c \cos\gamma_c} + K_{p_\psi} A_y \tag{47}$$

with ϕ_{ref} the output from the command filter discussed in section A, $V\cos\gamma_c$ the total airspeed in the horizontal plane, and A_y the body lateral acceleration. The derivation of this relationship is as follows. Consider the course angle dynamics, using the sum of forces in the lateral direction of the horizontal plane

$$mV_c \cos\gamma_c \dot{\chi}_c = \bar{Y}_b \cos\beta_c \cos\mu_c + L\sin\mu_c + F_T(\sin\alpha_c \sin\mu_c - \cos\alpha_c \cos\mu_c \sin\beta_c) \tag{48}$$

Here, $\bar{Y}_b$ is the aerodynamic side force in body frame and L the aerodynamic lift. We aim to bring the body side force $\bar{Y}_b$ to zero to achieve a coordinated turn. Furthermore, we neglect the effect of the thrust in the lateral direction so that $F_T \sin\beta_c \approx 0$, and the reference course rate for a coordinated turn is set to

$$\dot{\chi}_{c,ref} = \frac{1}{mV_c\cos\gamma_c}\left(L\sin\mu_c + F_T(\sin\alpha_c \sin\mu_c)\right) \tag{49}$$

in which an approximation of the vertical specific force can be substituted, because $mA_z \approx L + F_T \sin\alpha$. The calculation of the bank angle μ involves quite complex kinematics, although in practice and for the experiments considered in this paper it approximates the roll angle ϕ closely. Furthermore, the reference $\dot{\chi}_{c,ref}$ is set by the reference roll angle ϕ_{ref} instead of the state ϕ. In this way, the course rate reference *anticipates* for roll angle to be tracked. We are interested in finding a reference for $\dot{\psi}_{ref}$ instead of $\dot{\chi}_{ref}$. When there would be no wind, it holds that $\psi_{ref} = \chi_{ref}$, but with a constant wind, the aircraft heading deviates with a crab angle β_f, so that a reference for ψ_{ref} relates to the reference course angle by $\dot{\chi}_{ref} = \dot{\psi}_{ref} + \dot{\beta}_f$. A heading rate reference is therefore designed as

$$\begin{aligned}\dot{\psi}_{ref} &= \dot{\chi}_{c,ref} + \Delta\dot{\psi}_{ref} \\ &= \frac{mA_z \sin\phi_{ref}}{V_c\cos\gamma_c} + \Delta\dot{\psi}_{ref}\end{aligned} \tag{50}$$

with $\Delta\dot{\psi}_{ref}$ defined by a proportional control law on the side slip error. Hence with $\Delta\dot{\psi}_{ref} = K_p A_y$, we arrive at the result shown in Equation (47).

D. Angular acceleration estimation

Because no sensors for angular acceleration are available, the accelerations are estimated from the angular rates. This is done using a washout filter. It is shown previously in literature that the use of a washout filter is a simple way to obtain estimates of the angular accelerations that can be used for an incremental control law.[9,17] In discrete time the washout filter is implemented as

$$\begin{aligned}\boldsymbol{\omega}_f(k+1) &= \boldsymbol{\omega}_f(k) + T_s\omega_{n,w}\left[\boldsymbol{\omega}_m(k) - \boldsymbol{\omega}_f(k)\right] \\ \dot{\boldsymbol{\omega}}_f(k) &= \omega_{n,w}\left[\boldsymbol{\omega}_m(k) - \boldsymbol{\omega}_f(k)\right]\end{aligned} \tag{51}$$

with $\boldsymbol{\omega}_m = [p, q, r]_m^T$ the measured angular rates, $\boldsymbol{\omega}_f = [p, q, r]_f^T$ the filtered angular rates and $\dot{\boldsymbol{\omega}} = [\dot{p}, \dot{q}, \dot{r}]_f^T$ the filtered angular accelerations. $\omega_{n,w}$ denotes the bandwidth of the washout filter in $^{\text{rad}}/_{\text{s}}$, which has been set to $12\,^{\text{rad}}/_{\text{s}}$. It was determined minimizing by the phase lag caused by this filter while keeping acceptable noise levels on the final control surface commands.

E. Auto-throttle

During the experiments, executed maneuvers will have an immediate effect on the airspeed. However, it is desired to keep the airspeed at the same level during each executed experiment run, because the airspeed has a large effect on the aerodynamic effectiveness of each control surface. A proportional-control auto-throttle system is integrated in the flight software to keep airspeed within an acceptable range. The control law is

$$\delta_t = S_M\{\delta_{t,trim} + K_{p,t}(V_a - V_{a,trim})\} \tag{52}$$

where the *trim* point refers to the state at which the experiment run was started so that only differences are commanded with respect to the initial state. The saturation levels of the throttle command are $[0, 1]$. During the executed experiments, the control gain was set to $K_{p,t} = 0.15$. For the short experiments, an accurate velocity control is not needed. Therefore, no integrator control was added to the auto-throttle.

F. Controller gain tuning

Within the backstepping procedure, the only requirement that is imposed to provide asymptotic stability is that the gains C_1 and C_2 are positive definite. Gains C_1 and C_2 determine the behavior of the error dynamics $\mathbf{z}_1$ and $\mathbf{z}_2$, respectively. The gains have therefore been chosen such that the the cascaded loops are bandwidth limited. Since actuator dynamics are not considered as part of the plant during the control law derivation, the bandwidth of the inner loop must also respect the bandwidth of the actuators. Hence, the gains have been set such that $C_1 < C_2 < \boldsymbol{\omega}_{act}$. Small damping gains $C_{1,d}$ were added to reduce overshot in the roll and pitch mode. All gains are chosen manually using simulation results, but without additional optimization.

Table 4. Controller gains for body and aerodynamic attitude control

Aero			Body			
C_1	C_{1d}	C_2	C_1	C_{1d}	C_2	$\omega_{act}[^{\text{rad}}/_{\text{s}}]$
3	1	6	4	1.5	8	15.7
5	0	8	4	2	8	15.7
1	0	2	-	-	8	15.7

The remaining parameters in the control laws are the elements of $G_{2,0}$, which depend on the aerodynamic control derivatives as shown in Equation (16). To cancel the system dynamics and to force the error dynamics stable and decoupled, the best estimate of the real control effectiveness $G_{2,0}$ should be used. In Acquatella et al.[28] it is shown that INDI/IBS control laws can be compared with Proportional-Integral (PI) control. The proportional gain of such a control law is inversely proportional to the parameters of $G_{2,0}$. In this way it can be reasoned that IBS control laws can be configured to a more conservative setting by scaling $G_{2,0}$ with values greater than one, i.e., by overestimating the control effectiveness.

G. Incremental control loop with actuator position feedback

Reliable actuator position measurements were not available for closed-loop experiments. Therefore, actuator positions are estimated by modelling the actuators as a first-order linear system with rate limits, denoted by $\mathbf{A}(z)$:

$$\mathbf{u}(k+1) = \mathbf{u}(k) + T_s S_R\{\omega_{act}[\mathbf{u}_c(k) - \mathbf{u}(k)]\} \tag{53}$$

Here $\mathbf{u}_c$ are the commanded actuator positions. The parameters could be identified using open-loop step-response data. Time responses of the elevator deflections are shown in Figure 4. As can be seen, the proposed model is too simple for an accurate description of the dynamics in the operation domain. However, the model

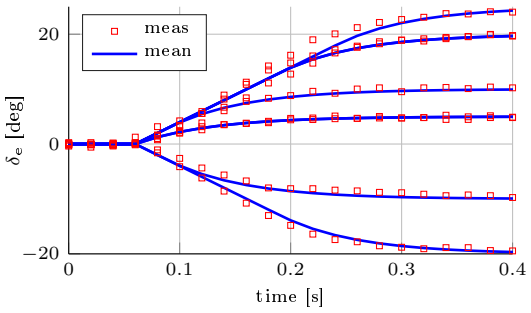

Figure 4. Measured elevator position (meas) for step commands and the simulated response using the final identified (mean) parameter estimates.

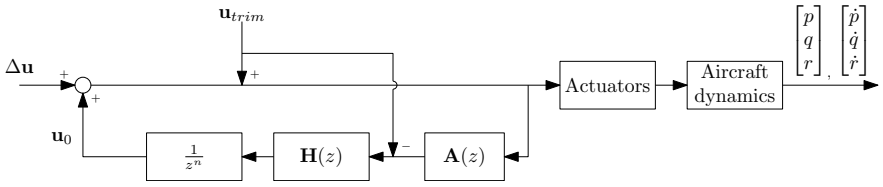

Figure 5. Incremental control loop with actuator model $\mathbf{A}(z)$, linear filter $\mathbf{H}(z)$ and delay.

yields a satisfactory result for the purpose of synchronization of $\mathbf{u}_0$ with the angular accelerations $\dot{\boldsymbol{\omega}}_f$. The final parameter estimates are $\omega_{act} = 2.35\,\text{Hz}$ and $R = 99.6\,^{\text{deg}}/_{\text{s}}$.

Furthermore, to synchronize the actuator feedback $\mathbf{u}_0$ with the angular acceleration feedback $\dot{\boldsymbol{\omega}}_0$, a controller time delay and a linear filter with the same bandwidth $\boldsymbol{\omega}_f$ as the washout filter has been incorporated in the incremental control loop (denoted by $\mathbf{H}(z)$). Finally, the controller command has been added to a constant initial command $\mathbf{u}_{trim}$, which corresponds to the last actuator commands before the controller is switched on. This ensures a smooth transition when switching from manual to automatic control in flight. An overview of the final incremental control loop is displayed in Figure 5.

H. Simulation and controller robustness

With the specified controller parameters for the loop gains, pre-filters, command-filters and total controller delay, series of simulations are performed to assess the robustness of the controllers. In these simulations, aerodynamic model parameters are varied by scaling the stability derivatives in various amounts between $0.75 \leq F \leq 1.25$. Simulations with only the inner loop angular rate tracking are also performed. Results of these simulations can be found in Figure 6. Steady state errors in the angular rate tracking response are due to non-negligible system dynamics increments $F_{2,0}\Delta\mathbf{x}$ (see Equation (17)). Smaller increment delays over which $\Delta\mathbf{u}$ acts decrease the effect of the system dynamics increments. This is shown by a second series of simulations with increased bandwidth of the actuators to 5 Hz and increased washout filter bandwidth to $24\,^{\text{rad}}/_{\text{s}}$. Results are plotted again in Figure 6. As can be expected, transient tracking responses are greatly improved due to increased bandwidth, but also the steady state tracking errors are considerably smaller.

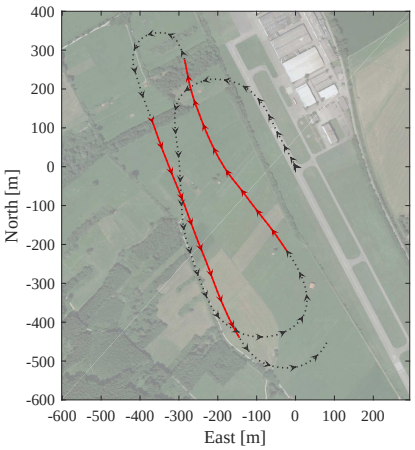

Figure 9. Trajectory of flight during the first two runs of experiment 1A.

Simulation results for the IBS body attitude controllers are presented in Figure 7. Simulation results of IBS aerodynamic attitude control laws are presented in Figure 8. The simulation results show that the system is highly robust to variations in model parameters.

V. Experiment set-up

The software with the designed control laws is implemented on the "Goldy flight control system (FCS)", of which the most important hardware components are listed in Table 5. The control laws run at a rate of 50 Hz. Before testing each of the control laws in flight, ground tests are performed to validate the software implementation and ensure a safe execution of the flight experiments.

Table 5. Aircraft avionics and hardware components

Component	Description
Flight Computer	Phytec MPC5200B Tiny (400 MHz, 64MB DDR DRAM, controller sample rate 50 Hz)
GPS Receiver	Novatel OEM Star
IMU	Analog Devices ADIS16405
Servos	DS8411 (1.55 Nm @4.8 V)
Pressure sensors	AMS5812

Each flight is manually controlled by an experienced safety pilot. During manual flight, speed is only roughly controlled by the throttle level. When the the aircraft is in a trimmed horizontal flight condition, the safety pilot switches from 'manual' to 'automatic' flight mode to initiate an experiment run. In automatic mode, the flight computer has complete control authority of all control surfaces. After about 6 - 12 seconds, the safety pilot switches back to manual flight. One flight can contain about 12 experiment runs.

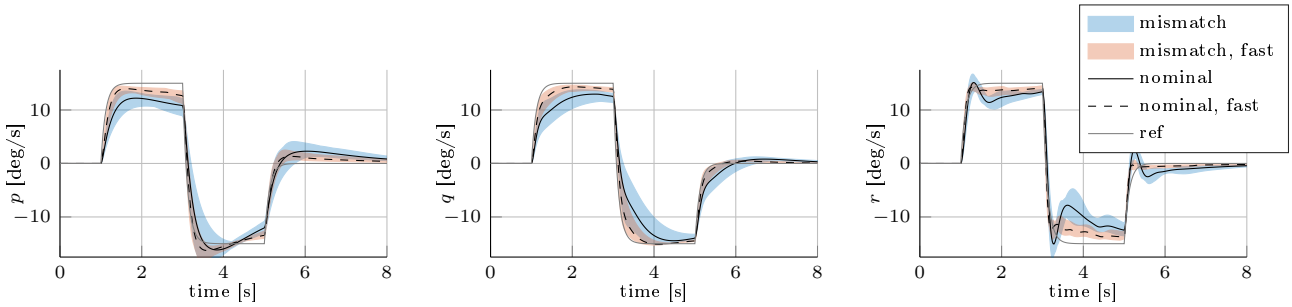

Figure 6. Tracking response of the inner angular rate incremental control loop, simulated separately for each different mode (roll/pitch/yaw), with the actual system specifications and with faster system specifications. Colored areas depict the simulated bounds with system dynamics model mismatches affecting both $\mathbf{f}_2$ and $\mathbf{g}_2$ by using aerodynamic parameter scaling factors $F_{i,\mathbf{base}}, F_{i,\mathbf{ctrl}}, F_{i,\mathbf{rate}} = 100\% \pm 25\%$.

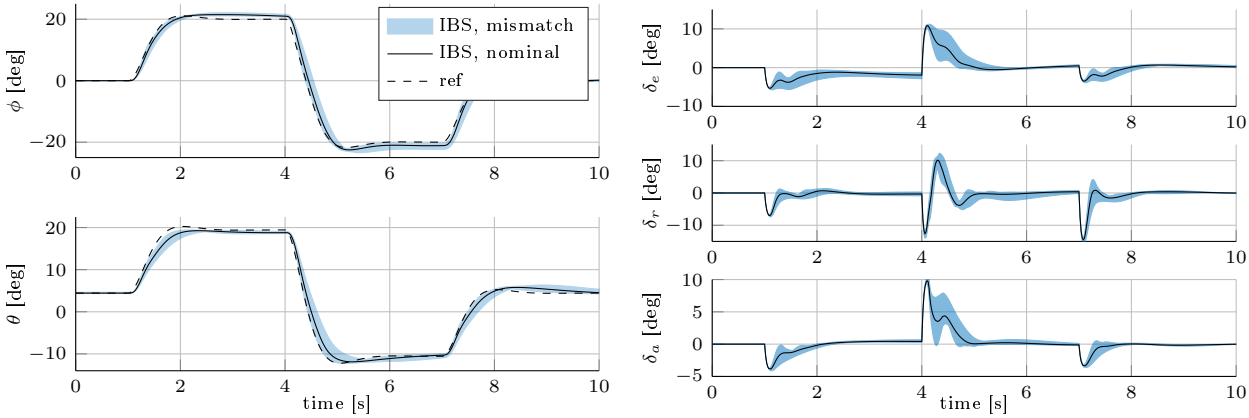

Figure 7. Tracking response with the IBS body attitude control laws. Colored areas depict bounds of the simulations with scaled aerodynamic control derivatives of $F_{i,\mathbf{ctrl}} = 100\% \pm 25\%$

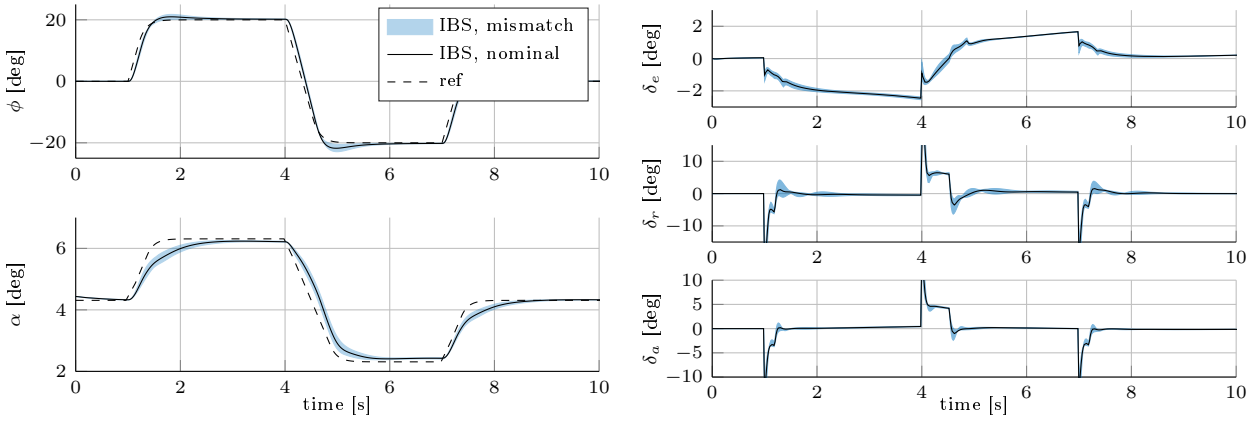

Figure 8. Tracking response with the IBS aerodynamic attitude control laws. Colored areas depict bounds of the simulations with scaled aerodynamic control derivatives of $F_{i,\mathbf{ctrl}} = 100\% \pm 25\%$

Table 6. List of sequentially executed experiments

#	Controller configuration	Tracking tasks
Body attitude control experiments		
1A	Pitch control only, manual roll/yaw and velocity control (conservative parameters)	Pitch angle doublets (± 10 deg)
1B	Add auto-throttle control	Pitch angle doublets (± 10 deg)
1C	Add roll/yaw control (fully automatic control)	Roll angle doublets ($\pm 20, \pm 30$ deg)
2	Fully automatic control, nominal gains	Pitch angle doublets ($\pm 10, \pm 15$ deg) Roll angle doublets ($\pm 20, \pm 45$ deg)
3	Augmented manual control	Pilot commands
Aerodynamic attitude control experiments		
4	Pitch and velocity control only, manual roll/yaw control (conservative parameters)	α doublets ($\pm 1, \pm 2$ deg)
5	Pitch and velocity control only, manual roll/yaw control, nominal gains	α doublets ($\pm 1, \pm 2$ deg)
6	Add roll/yaw control (fully automatic control). Conservative gains in the lateral modes.	Roll angle doublets (± 15 deg)

Figure 10. The FASER aircraft during one of the experiments.

Each experiment consists of a controlled maneuver, during which a specific part of the control laws is tested. In all cases, the attitude commands $\phi_{ref}, \theta_{ref}, \alpha_{ref}$ are either pre-programmed inputs *or* inputs directly commanded from the remote pilot control. The pre-programmed inputs are always doublets to test positive and negative step responses. The different experiments that have been executed are listed in Table 6. Each experiment defines a different controller configuration. Within each experiment, different tracking tasks are executed. Before nominal controller settings were applied, experiments were performed with more conservative settings (experiment 1A, 1B, 1C, 4). The conservative parameters are defined by a scaling of the estimated control effectiveness parameters $G_{2,0}$ by a factor 2. Also, the first few runs of every experiment in Table 6 consist of a simple stabilization task in which the initial attitude needs to be held. When stable responses are observed, doublet signals with increasing magnitude are commanded in the subsequent tasks of most experiments. During the last flight of the body attitude control experiments, the control law is used as an augmented control law in which the pilot gives commands for the roll and pitch angle that are tracked by the control system. The experiments are all done for multiple runs, at flight speeds between 20 and 35 $^{\mathrm{m}}/_{\mathrm{s}}$ and between 100 and 200 m above ground. On total, a number of 68 successfully controlled runs are flown. As an example, Figure 9 shows the horizontal flight trajectory of the flight in which experiments 1A and 1B were executed.

The following two notes concerning the experiment execution of the experiments with the IBS aerodynamic attitude flight controller must be made:

1. During experiments 1, 2 and 3 with the body attitude controller, the feed-forward term $G_1^T \mathbf{z}_1$ was not included in the control law. This makes the control law identical to a multi-loop nonlinear dynamic inversion control law as discussed in section 2. This term is very small and should have a minimal effect on the closed-loop response of these experiments. This choice was made to build up the complexity of the tested control laws over all experiments. In experiments 4,5 and 6, the full backstepping control laws including this term have been used in the more complex aerodynamic attitude control law.

2. The lateral mode of the aerodynamic attitude controller was only tested with conservative parameters in the roll angle feedback. Furthermore, in the aerodynamic attitude controller experiments, a simplified sideslip control was used. The sideslip control was a simple proportional control added to the yaw rate command, with a feedback from the measured lateral acceleration. Therefore, the value of the flight results of the lateral mode is limited.

An on-board camera was mounted on the vertical tail to capture all experiments. Videos are uploaded and

publicly available.[a] Figure 10 shows a movie frame as an example.

VI. Results

A. Body attitude control flight results

During the execution of experiments 1-3 (see Table 6), a total of 44 successful runs lasting about 10 seconds each have been flown with the presented body attitude controller. In Figures 11 and 12, flight data of the pitch angle tracking responses are shown. Roll angle tracking results are shown in Figures 13 and 14. A manually controlled flight with augmented INDI controller was performed and lasted in total 241 seconds. Results of a typical part of the flight are shown in Figure 15. All runs resulted in stable and accurate responses with a low tracking error, matching our expectations from simulation results.

One can see that the simulation response matches well with the response measured in-flight. The elevator input is slightly less damped in simulation. This indicates an underestimation of the pitch damping in the model. Looking at the aileron input for the lateral experiments, this difference is not visible. However, by looking at the angular rate response, these experiments show relatively more effects from disturbances. Disturbances from turbulence are not simulated here.

The root mean square (RMS) of the tracking errors are shown in Figure 19. The experiments with nominal parameters show a low overall error, following the same trends as observed in simulation. In flight, the RMS error is slightly larger for all experiments. In the time responses, this difference is visible by a slight delayed tracking response.

Overall, the results clearly show that the flight control laws function well over a variety of airspeeds ($V > 20\,\mathrm{m/s}$). Figure 11 shows that at lower speeds the elevator inputs contain more oscillations due to a decreased elevator effectiveness. Due to the variety of airspeeds that are tested and the two different parameter settings (nominal and conservative) that are chosen, the results demonstrate that the controller is able to follow the specified reference with desired error dynamics.

B. Aerodynamic attitude control flight results

For experiments 4 and 5 (see Table 6), on total 22 runs each of about 10 seconds were executed. Results of the longitudinal tracking of the aerodynamic attitude controller are shown in Figures 17 and 18. Results of the lateral aerodynamic attitude control with conservative parameters and simplified sideslip controller are shown in Figure 16. RMS tracking errors can be found in Figure 19.

A clear tracking of the reference α_{ref} is visible. The results show that the controller functions well between airspeeds of 25 and 35 $\mathrm{m/s}$. Furthermore, the observed response in-flight matches with the simulation results. The difference in RMS error between simulation and flight can be partly attributed to the additional turbulence and vibrations measured in flight which was not included in simulation. As can be seen in the results, especially when tracking doublets with a magnitude of 1 deg, the variance of the turbulence is quite big compared to the reference signal. Nevertheless, the observed effect of the turbulence propagating in the elevator deflection is small, the response is stable and damped and tracking is fast.

An issue with using the unfiltered estimate of α is that upon initiation of the controller, the angle of attack reference α_{ref} is set to its actual estimate which includes the measured turbulence and vibrations mainly coming from the motor and propeller. This results in tracking a non-zero vertical load as reference offset and causes the aircraft to follow this reference, thereby initially pitching either up or down. This effect can be seen in the pitch angle response in Figures 17 and 18. Although this can and should normally be prevented by using alternative estimates of α, the results still show the corrected tracking of the the reference.

Looking at the roll angle response in Figure 16, a clear tracking is observed. Since conservative parameters are used for this mode and since the damping parameter $C_{1,d}$ was set to zero, the response is slow and contains overshoot. Simulation results match closely with the observed response. The yaw rate response and the rudder input (not shown here) contained oscillations that were only marginally damped.

Overall, the responses show that the aerodynamic attitude controller follows the imposed dynamics and performs as expected. Especially the longitudinal mode is showing that the controller can be used for stable, accurate tracking of an imposed reference signal.

[a] A selection of the experiment runs can be viewed at `https://youtu.be/NJN3Q4PwTxo`.

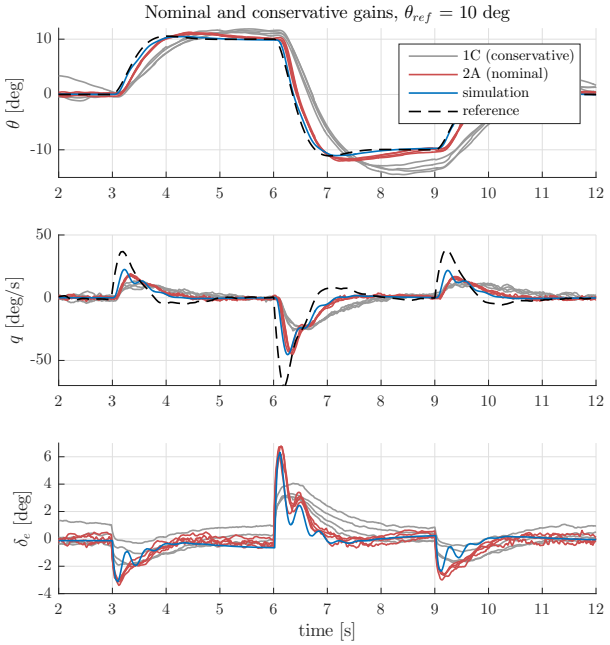

Figure 11. Body attitude control, experiment 1B and 2. Longitudinal tracking response for pitch angle commands of 10 deg, showing pitch angle, pitch rate and elevator deflection. Pitch angles and elevator deflections are deviations from the initial state.

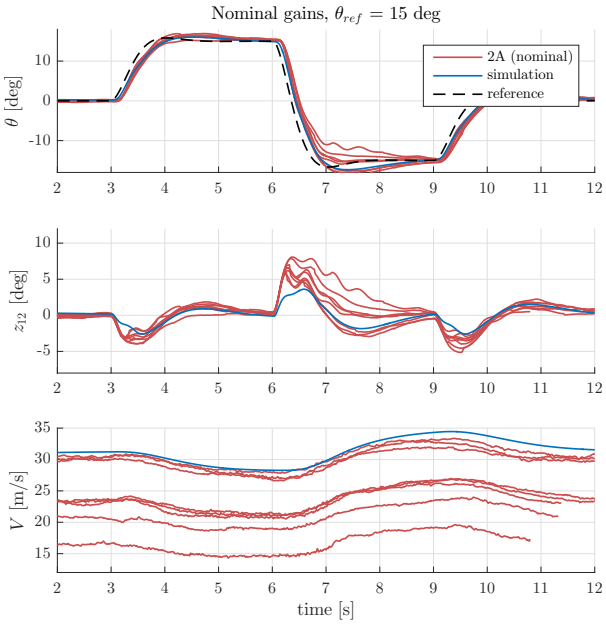

Figure 12. Body attitude control, experiment 2. Longitudinal tracking response for pitch angle commands of 15 deg, showing pitch angle, tracking error and airspeed. Pitch angles are deviations from the initial state.

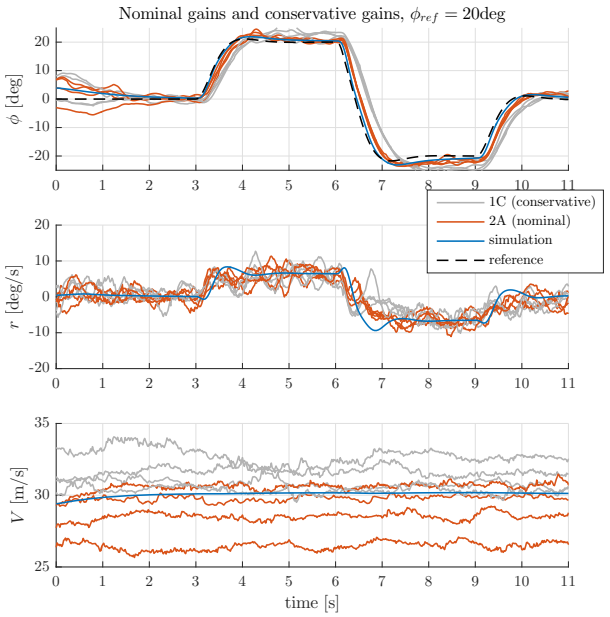

Figure 13. Body attitude control, experiment 1C and 2. Lateral tracking response, with roll angle commands of 20 deg, showing roll angle, yaw rate and airspeed.

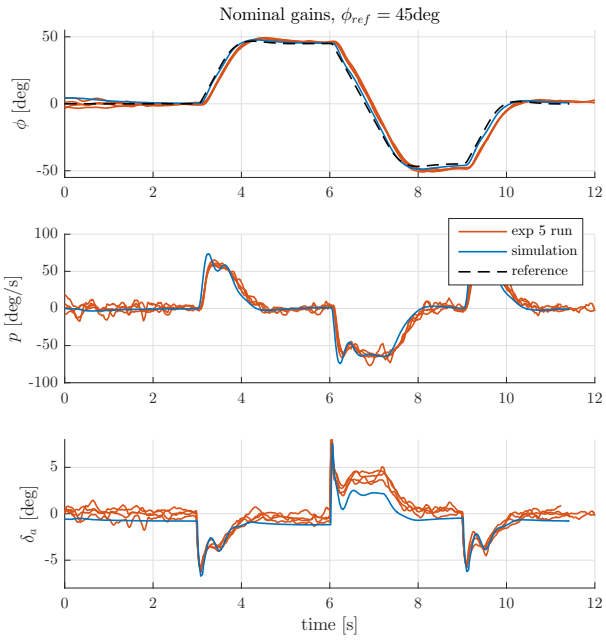

Figure 14. Body attitude control, experiment 2. Lateral tracking response, with roll angle commands of 45 deg, showing roll angle, roll rate and aileron deflection.

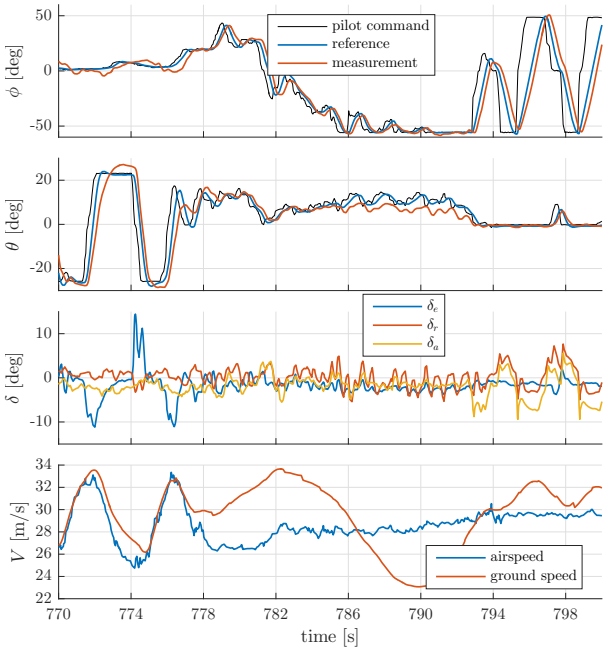

Figure 15. Body attitude control, experiment 3. Tracking response of augmented manual flight. Pitch angles and control deflections are deviations from the initial state.

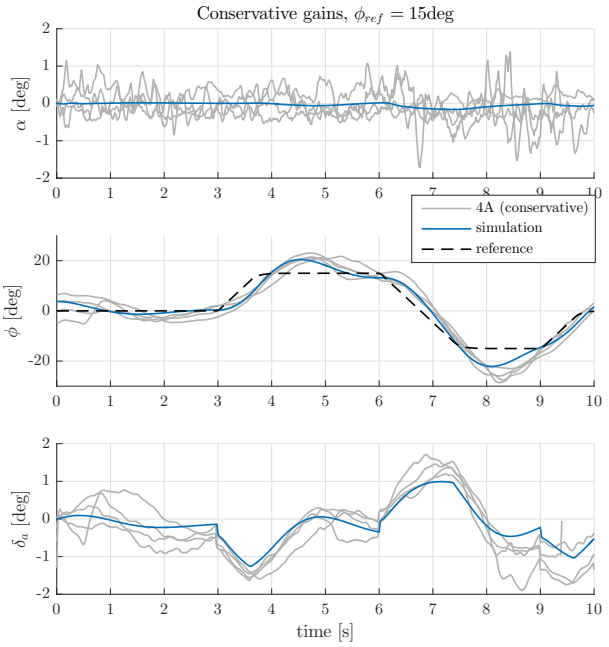

Figure 16. Aerodynamic attitude control, experiment 6. Lateral tracking response with conservative parameters only, comparing flight data and simulated data, with roll angle commands of 15 deg. Aileron deflections are deviations from the initial value.

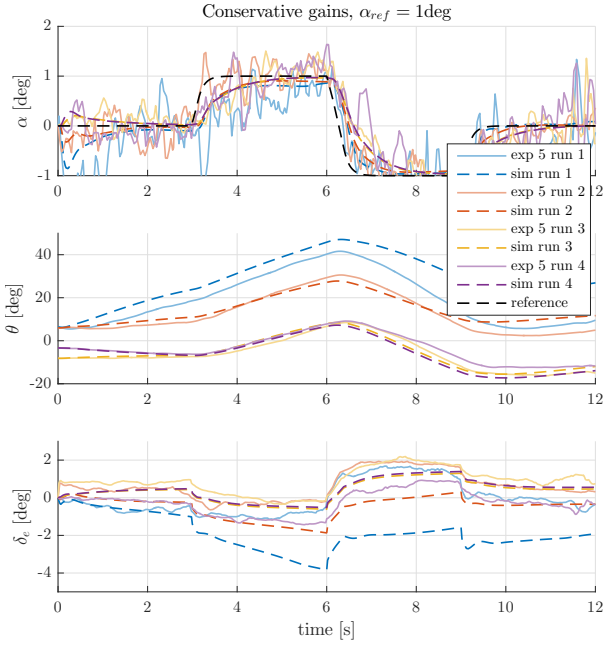

Figure 17. Aerodynamic attitude control, experiment 4 and 5. Longitudinal tracking response, comparing flight data with simulations. α commands of 1 deg with both nominal and conservative parameters are plotted, showing angle of attack, pitch angle and elevator deflection. Angles of attack and control surface deflections are deviations from the initial state.

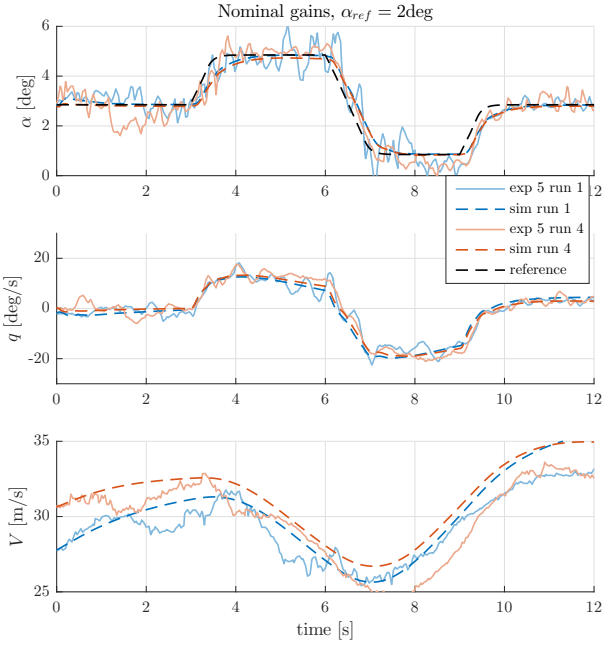

Figure 18. Aerodynamic attitude control, experiment 5. Longitudinal tracking response, comparing flight data with simulations. α commands of 2 deg with nominal parameters are plotted, showing angle of attack, pitch rate and airspeed. Angles of attack are deviations from the initial state.

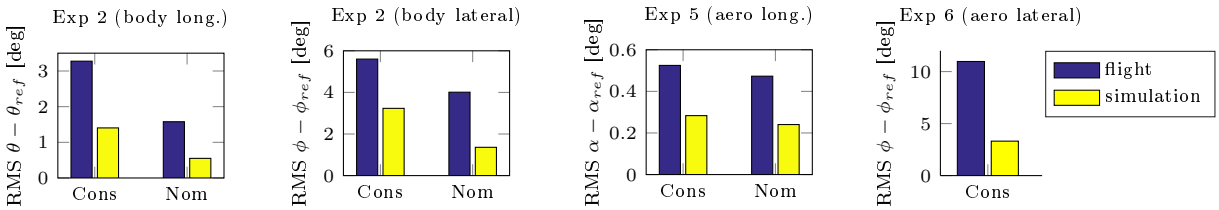

Figure 19. RMS tracking error results over all runs of the separate experiments with the body attitude controller and aerodynamic attitude controller.

VII. Conclusion

The paper presents the design, implementation and flight test of IBS for the attitude stabilization and control of a fixed-wing aircraft. The resulting control laws are very similar to multi-loop incremental nonlinear dynamic inversion control laws, but are derived using the Lyapunov stability framework. Qualitative flight tests are performed to validate simulation results presented in this paper and shown in previous studies on incremental nonlinear flight control methods.[7,17] In particular, a successful application of command-filtered IBS methods on a fixed-wing aircraft are shown on a UAV that contains relatively cheap and widely available avionics components and actuators. This was not done before in practice. By implementing control laws for controlling body attitude angles and aerodynamic attitude angles, we showed the applicability of these control laws for manual augmented attitude control, outer loop flight path control and vertical load control.

Through repeated experiments, flight data results of the IBS attitude controllers show that accurate tracking is achieved and system dynamics are canceled well without requiring much knowledge of model parameters. Simulation results with identical controller configurations match closely with the observed response. Hence, the results in this paper validate the applicability of the control methods under the presence of parameter uncertainties, delayed measurements and disturbances.

Control laws proposed in this paper require little knowledge about the system dynamics, yet they result in an asymptotically stable system by being more dependent on sensor measurements. The simplicity of the resulting control law makes it easy to implement. Advantages compared to classical methods are that they are easy to tune and propose one control design that is valid over the entire flight envelope. Compared to modern alternatives, IBS shows to be an attractive flight control law for future high-performance, fault-tolerant flight control systems.

Acknowledgements

We highly appreciate the contribution made by Andreas Klöckner, Nir Kastner, and Reiko Müller at the institute of System Dynamics and Control at DLR, to the execution of experiments on the FASER UAV.

References

[1]Dale, E., Dan, B., Russ, H., and Gunter, S., "Dynamic inversion: an evolving methodology for flight control design," *International Journal of Control*, Vol. 59, No. 1, 1994, pp. 71–91.

[2]Bordignon, K. and Bessolo, J., "Control Allocation for the X-35B," *AIAA Biennial International Powered Lift Conference and Exhibit, Aviation Technology, Integration, and Operations (ATIO)*, 2002.

[3]Goupil, P., Boada-Bauxell, J., Marcos, A., Cortet, E., Kerr, M., and Costa, H., "AIRBUS efforts towards advanced real-time Fault Diagnosis and Fault Tolerant Control," *IFAC Proceedings Volumes*, Vol. 47, No. 3, 2014, pp. 3471 – 3476, 19th IFAC World Congress.

[4]Goupil, P. and Marcos, A., "Advanced Diagnosis for Sustainable Flight Guidance and Control: The European ADDSAFE Project," *SAE Technical Paper*, SAE International, 10 2011.

[5]Bacon, B. J., Ostroff, A. J., and Joshi, S. M., "Reconfigurable NDI Controller Using Inertial Sensor Failure Detection & Isolation," *Aerospace and Electronic Systems, IEEE Transactions on*, Vol. 37, No. 4, 2001, pp. 1373–1383.

[6]Smith, P. R., "A Simplified Approach to Nonlinear Dynamic Inversion Based Flight Control," *AIAA Atmospheric Flight Mechanics Conference and Exhibit*, 1998, pp. 762–770.

[7]Sieberling, S., Chu, Q. P., and Mulder, J. A., "Robust Flight Control Using Incremental Nonlinear Dynamic Inversion and Angular Acceleration Prediction," *Journal of Guidance, Control, and Dynamics*, Vol. 33, No. 6, 2010, pp. 1732–1742.

[8]Simplício, P., Pavel, M. D., van Kampen, E., and Chu, Q. P., "An Acceleration Measurements-Based Approach For

Helicopter Nonlinear Flight Control Using Incremental Nonlinear Dynamic Inversion," *Control Engineering Practice*, Vol. 21, No. 8, 2013, pp. 1065–1077.

[9]Smeur, E. J. J., Chu, Q. P., and de Croon, G. C. H. E., "Adaptive Incremental Nonlinear Dynamic Inversion for Attitude Control of Micro Aerial Vehicles," *Journal of Guidance, Control, and Dynamics*, Vol. 39, No. 3, 2016, pp. 450–461.

[10]Acquatella B., P., Falkena, W., van Kampen, E., and Chu, Q. P., "Robust Nonlinear Spacecraft Attitude Control using Incremental Nonlinear Dynamic Inversion," *AIAA Guidance, Navigation, and Control Conference*, , No. August, 2012.

[11]Lu, P., van Kampen, E., de Visser, C. C., and Chu, Q. P., "Aircraft Fault-Tolerant Trajectory Control Using Incremental Nonlinear Dynamic Inversion," *Control Engineering Practice*, Vol. 57, 2016, pp. 126–141.

[12]Acquatella B., P., van Kampen, E., and Chu, Q., "Incremental Backstepping for Robust Nonlinear Flight Control," *Proceedings of the EuroGNC 2013, 2nd CEAS Specialist Conference on Guidance, Navigation & Control*, 2013, pp. 1444–1463.

[13]Acquatella B., P., *Robust Nonlinear Spacecraft Attitude Control: An Incremental Backstepping Approach*, MSc thesis, Delft University of Technology, 2011.

[14]Ali, A. A. H., Chu, Q. P., van Kampen, E., and de Visser, C. C., "Exploring Adaptive Incremental Backstepping using Immersion and Invariance for an F-16 Aircraft," *AIAA Guidance, Navigation, and Control Conference*, 2014.

[15]Dong, W., Farrell, J. A., Polycarpou, M. M., Djapic, V., and Sharma, M., "Command Filtered Adaptive Backstepping," *IEEE Transactions on Control Systems Technology*, Vol. 20, No. 3, 2012.

[16]Sonneveldt, L., Chu, Q. P., and Mulder, J. A., "Nonlinear Flight Control Design Using Constrained Adaptive Backstepping," *Journal of Guidance, Control, and Dynamics*, Vol. 30, No. 2, 2007, pp. 322–336.

[17]van Gils, P., van Kampen, E., de Visser, C. C., and Chu, Q. P., "Adaptive Incremental Backstepping Flight Control for a High-Performance Aircraft with Uncertainties," *AIAA Guidance, Navigation, and Control Conference*, 2015.

[18]Vlaar, C. M., *Incremental Nonlinear Dynamic Inversion Flight Control*, MSc thesis, Delft University of Technology, 2014.

[19]Berry, A. and Smith, P., "Flight Test Experience of a Non-linear Dynamic Inversion Control Law on the VAAC Harrier," *AIAA Atmospheric Flight Mechanics Conference*, 2000, pp. 132–142.

[20]Owens, B., Cox, D. E., and Morelli, E. A., "Development of a Low-Cost Sub-Scale Aircraft for Flight Research: The FASER Project," *AIAA Aerodynamic Measurement Technology and Ground Testing Conference*, 2006, pp. 1–11.

[21]Hoe, G., Owens, D. B., and Denham, C., "Forced Oscillation Wind Tunnel Testing for FASER Flight Research Aircraft," *AIAA Atmospheric Flight Mechanics Conference*, 2012, pp. 1–12.

[22]Farrell, J., Sharma, M., and Polycarpou, M., "Backstepping-Based Flight Control with Adaptive Function Approximation," *Journal of Guidance, Control, and Dynamics*, Vol. 28, No. 6, 2005, pp. 1089–1102.

[23]Sonneveldt, L., *Adaptive Backstepping Flight Control For Modern Fighter Aircraft*, PhD Thesis, Delft University of Technology, 2010.

[24]van Gils, P., *Adaptive Incremental Backstepping Flight Control*, MSc thesis, Delft University of Technology, 2015.

[25]Krstić, M., *Nonlinear and Adaptive Control Design*, Wiley, 1995.

[26]Astolfi, A. and Ortega, R., "Immersion and Invariance: A New Tool for Stabilization and Adaptive Control of Nonlinear Systems," *IEEE Transactions on Automatic Control*, Vol. 48, No. 4, 2003, pp. 590–606.

[27]Sonneveldt, L., van Oort, E., Chu, Q. P., and Mulder, J., "Immersion and Invariance Based Nonlinear Adaptive Flight Control," *AIAA Guidance, Navigation, and Control Conference*, , No. August, 2010.

[28]Acquatella B., P., van Ekeren, W., and Chu, Q. P., "PI(D) tuning for Flight Control Systems via Incremental Nonlinear Dynamic Inversion," *20th International Federation of Automatic Control (IFAC) World Congress*, 2017.